NORTH SEA FLOW MEASUREMENT WORKSHOP
measuring for the energy transition

Multiphase Metering Using a Dual Frequency Coriolis Mass Flow Meter

Sakethraman Mahalingam, Aramco Overseas Company
Hao Zhu, Endress + Hauser Flow
Liyun Lao, Cranfield University

1 INTRODUCTION

Coriolis meters are used on the liquid line coming out of many first-stage separators to measure the mass flow rate of the produced hydrocarbon liquid. In addition to the mass flow rate, the liquid density from the meter is conveniently interpreted as a water-cut measurement. However, given that many of these separators are at least a decade old, they are often operating outside of their design specifications and may have gas carry-under issues. In many cases, the Gas Volume Fraction (GVF) may be as much as 25% on the liquid line while they are designed to have less than 1% GVF. Unfortunately, many of Coriolis meters on these separators today are unable to tolerate a GVF of even 5%. When most of the time, the gas is present as free bubbles, in some cases, it may be trapped within the oil. There is a big need for getting accurate and reliable flow measurements from these facilities to enable proper reservoir management [1].

The cost of replacing separators and other such equipment involves significant capital costs. In the short and medium term, it may be best if the Coriolis meter is replaced with a more gas-tolerant meter that can continue to provide a meaningful mass flow rate. Many modern Coriolis meters are able to handle increasing amounts of entrained gas but there is a still a long way to go before they are accepted by operators. In this paper, the results from the testing of a dual-frequency Coriolis meter under multiphase conditions are reported.

2 MULTI-FREQUENCY CORIOLIS METER TECHNOLOGY

One of the exciting new advances in Coriolis meter technology is the oscillation of flow tubes at multiple frequencies [2] [3]. While Coriolis flowmeters are traditionally driven at the natural resonance frequency, there are additional natural modes associated with the system in addition to the primary mode. With Multi-Frequency Technology (MFT), the tubes are also driven at their third natural mode. By analyzing the signals filtered at this different frequency, one can obtain additional information about the vibrational properties of the fluid, and compensate the measurement errors caused by the compressibility of an entrained gas fluid.

Some recent research [4] has discovered that different types of gas bubbles, namely free bubbles and suspended bubbles, have different impact on the meter performance. It is also crucial to identify the bubble pattern in the measuring tube of a Coriolis meter to make a diagnosis and reduce the negative influence of the disturbance accordingly. To realize this, Gas Fraction Handler (GFH) software from Endress+Hauser has been developed for Coriolis meters [5].

Fig. 1 – Multi-Frequency Coriolis Meter

3 TEST PROGRAM

An experimental program was conducted at the 2-inch multiphase flow loop at Cranfield University. Fig. 2 shows a photo of the Process Engineering Laboratory at Cranfield University and the 2-inch vertical flow line is at the left of the picture. The test meter was installed approximately at 5.5m from the ground level and the total height of the vertical section is about 11m.

The meter was installed in a "flag" position as shown in Fig. 3 as advised by the manufacturer [5]. The flow loop was capable of pumping up to 40m^3/hour of oil or water and up to 75m^3/hour of air (under standard conditions). The oil used was Rustlick EDM 250 dielectric oil with a density of 810kg/m^3 and a viscosity of 7.2mPa.s at 21^{o}C. Air was treated as an ideal gas with a density of 1.225kg/m3 under standard conditions. The density of water was taken as 1002 kg/m3 under standard conditions.

Fig. 2 – Process Engineering Laboratory – Cranfield University

Fig. 3 – Meter Under Test in "Flag" Position

A test matrix comprising of five water-cuts – 0%, 30%, 50%, 70% and 100%, liquid flow rates between 5 and 35 m^3/hour and an air flow rates between 2 and 75 m^3/hour (under standard conditions) was developed. A total of 204 unique test points covered a GVF range from 0% to 70%. About 50% of the test points corresponded to the bubbly flow regime and the remaining points were in the slug flow regime.

3 TEST RESULTS

3.1 Measurements Under Water-Oil Flow

The meter was tested under liquid flow to establish the baseline for the multiphase testing. Fig.4 and Fig. 5 show the plot of density and mass flow from the meter across all water-cuts. Given the uncertainty in the flow loop is about 1%, the meter under test performed well within this uncertainty level.

3.2 Measurements Under Flow with Gas

As the amount of gas injected into the flow was increased, the density reported by the meter decreased, consistent with expectations. The meter was able to provide a density up to 50% GVF though at GVF greater than 20%, there was increased scatter of up to 8% in the reported density (Fig. 6).

The scatter in the reported mass flow rate was higher (up to 25%) at GVF greater than 15% while it was below 5% at GVF less than 15% (Fig. 7). The scatter in mass flow depends not only on the GVF but also the liquid density and liquid flow rate. Hence the data presented in Fig. 7 must not be interpreted too simplistically as it shows the relationship of the scatter in mass flow measurements only to GVF.

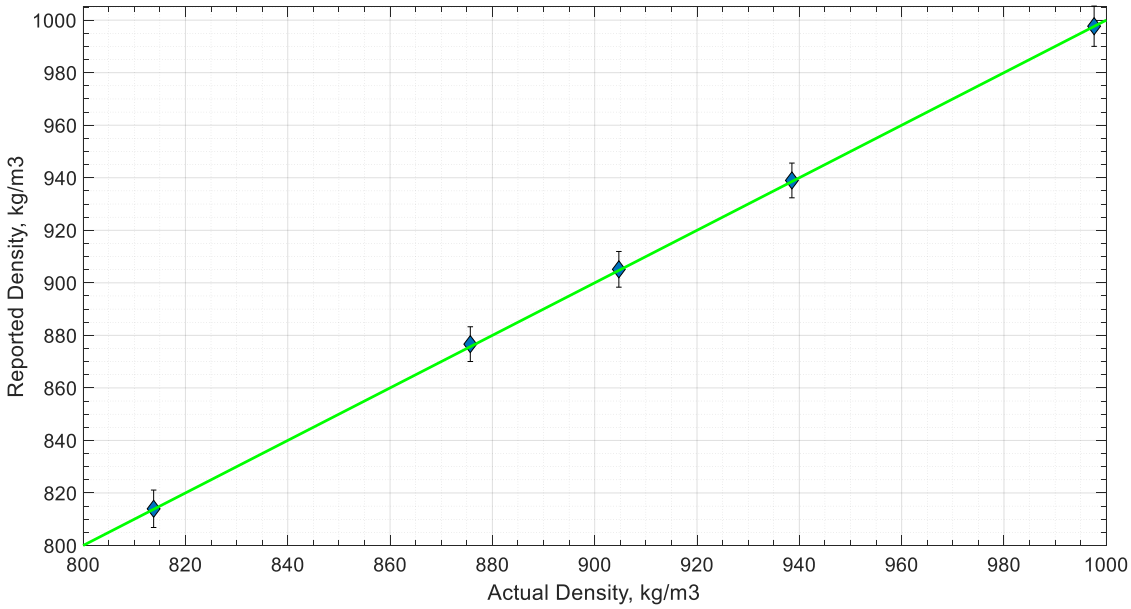

Fig. 4 – Density Measurements from the Meter under 0% GVF

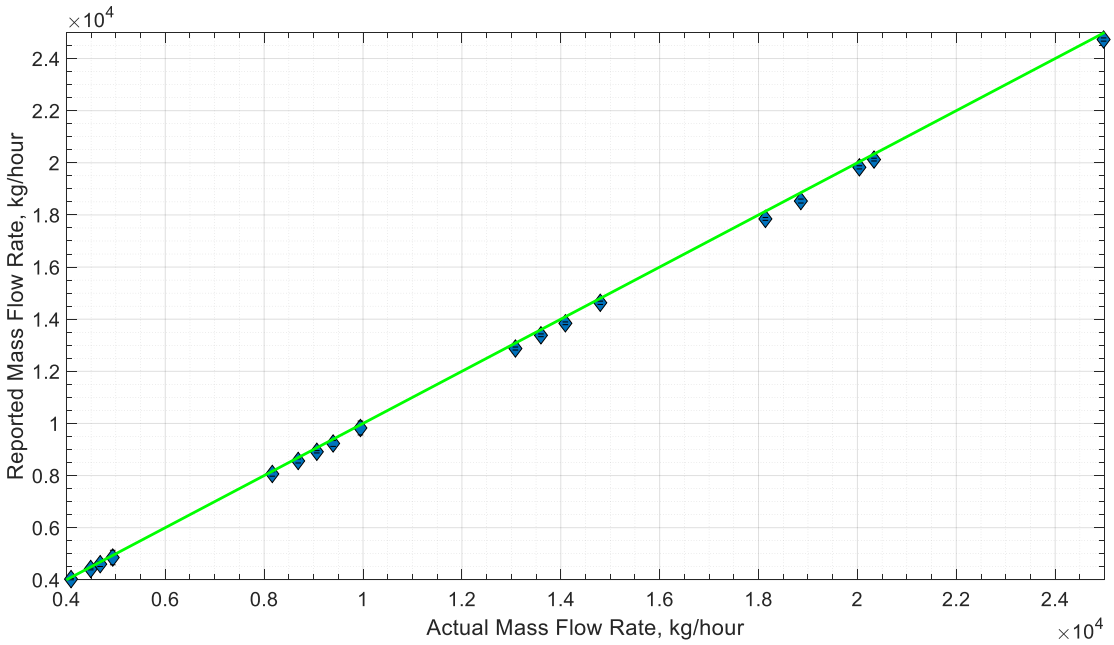

Fig. 5 – Mass Flow Measurements from the Meter under 0% GVF

It is also important to consider that scatter is not only a function of the meter's performance but also of the uncertainty in the flow loop. It is expected that at higher GVF, it is likely that the flow at entry of the meter was in the slug flow regime. Given the pressure drop that occurred across the meter, it is likely that the GVF increased within the meter. The scatter in the meter increases as there may be no one true GVF at the meter under these conditions, the presented value is merely an average GVF based on the average pressure at the meter.

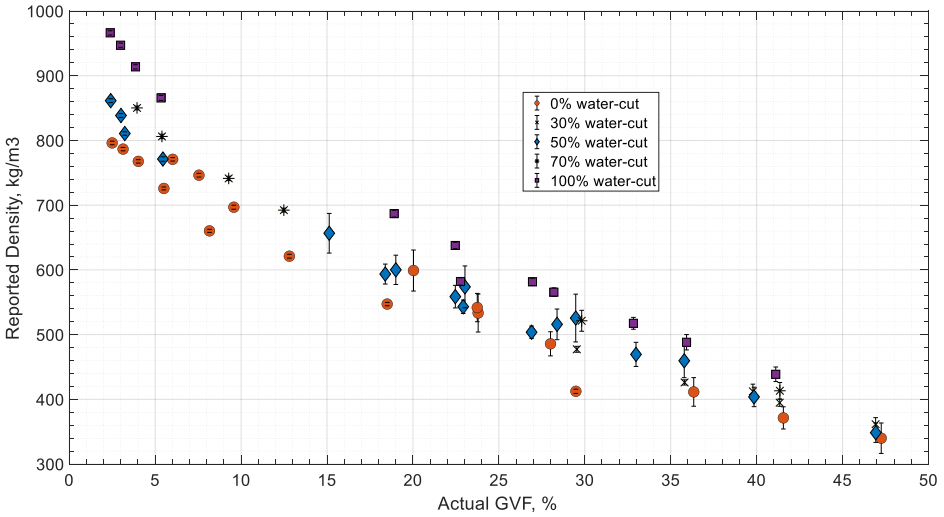

Fig. 6 – Reported Density Vs. Gas Volume Fraction

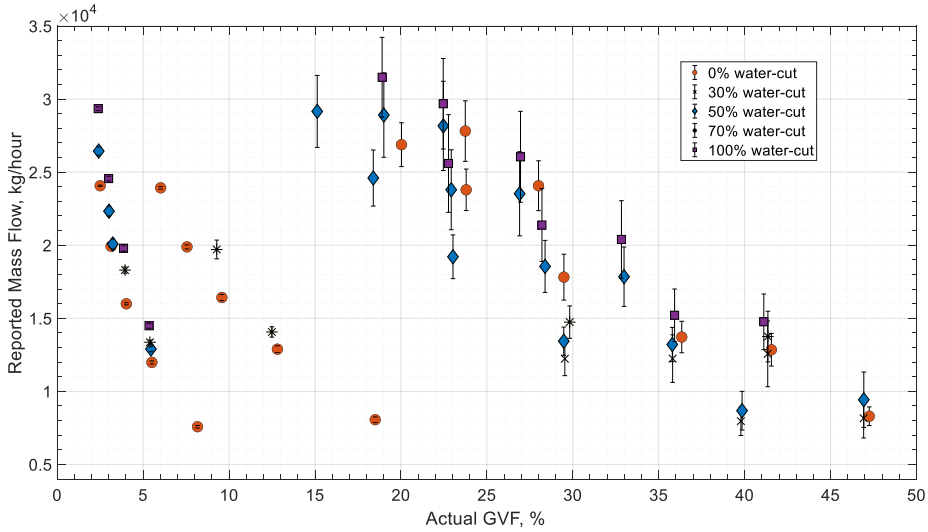

Fig. 7 – Reported Mass Flow Vs. Gas Volume Fraction

3 ERRORS IN CORIOLIS METERS

Hemp [6] described a theoretical framework for understanding the two main sources of errors in Coriolis meters with entrained gas - phase decoupling and compressibility. Phase decoupling (also called the bubble effect) errors occur due to the physical decoupling of the gas phase from the vibration response of the liquid phase due to buoyancy. This results in a shift in the center of mass of the fluid with respect to the center of mass of the tube. As described by Basse [7], the phase decoupling error tends to always be negative. The error due to compressibility of the gas phase (also referred to as resonator effect [2] [3]) occurs when the gas bubbles gets compressed against the outer walls of the tube by the heavier liquid [6] [8]. This causes a larger than expected reaction force on the tube and tends to result in overestimation of the measured parameters. Hence compressibility always causes a positive error in both density and mass flow rate.

According to Hemp [6], the error in density and mass flow rate in a Coriolis meter entrained with gas is given by equations (1) and (2) as given below. These equations apply for a gas of zero density entrained in an inviscid liquid. The first term in both equations is the error due to phase decoupling and the second term is related to the compressibility of the gas.

$$E_d = \frac{-2\alpha}{1-\alpha} + \frac{1}{4}\left[\frac{w_1 b}{c}\right]^2 \quad (1)$$

$$E_m = \frac{-2\alpha}{1-\alpha} + \frac{1}{2}\left[\frac{w_1 b}{c}\right]^2 \quad (2)$$

3.1 Error Modelling for Density

The error in density may be modelled using the Hemp's approach. It is important to note that in Eqn. (3), the phase decoupling term (the first term) is at least 100 times larger than the compressibility term (the second term) for an entrained gas fluid with free bubbles. Hence the error in density always tends to be negative and strongly a function of decoupling. In fact, experimental results indeed show this trend (Fig. 8). As shown in Fig. 8, the slope of the error in density with respect to GVF is between -0.65 and -1.1 and is much smaller than predicted by Hemp. This is to be expected because the gas density is non-zero and liquid has a non-zero viscosity. Higher the density of the gas, lower the bubble effect and similarly, higher the viscosity of the liquid, the lower the decoupling tendency of the gas. Furthermore, the phase decoupling effect may not be fully valid for slug flow pattern.

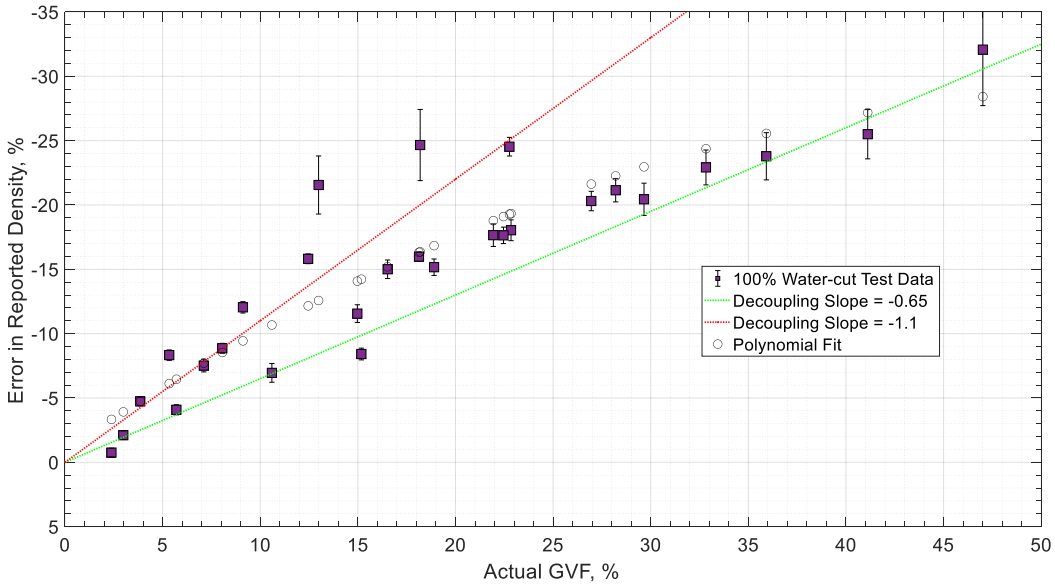

Fig. 8 – Error in Reported Density Vs. Gas Volume Fraction for 100% Water-Cut

Indeed, it is possible to turn the reported density into a calculated GVF by assuming that the liquid density is known through a water-cut meter. Fig. 9 shows the calculated GVF vs actual GVF for all water-cuts. It is clear that the GVF tends to be overestimated because the reported density is always lower that the actual mixture density. The error in calculated GVF for 0% water-cut is slightly smaller than the rest of the water-cuts – again, this may be due to the higher viscosity of the oil.

By simply using a straight line or a second order polynomial fit through the data in Fig. 9, it is possible to get a decent model to predict GVF from measured density (if the water-cut is known). While the relationship seems to be a function of water-cut, it seems to be almost independent of liquid flow rate. However, it is possible that this may change at much higher flow velocities or under different pressure/temperature conditions.

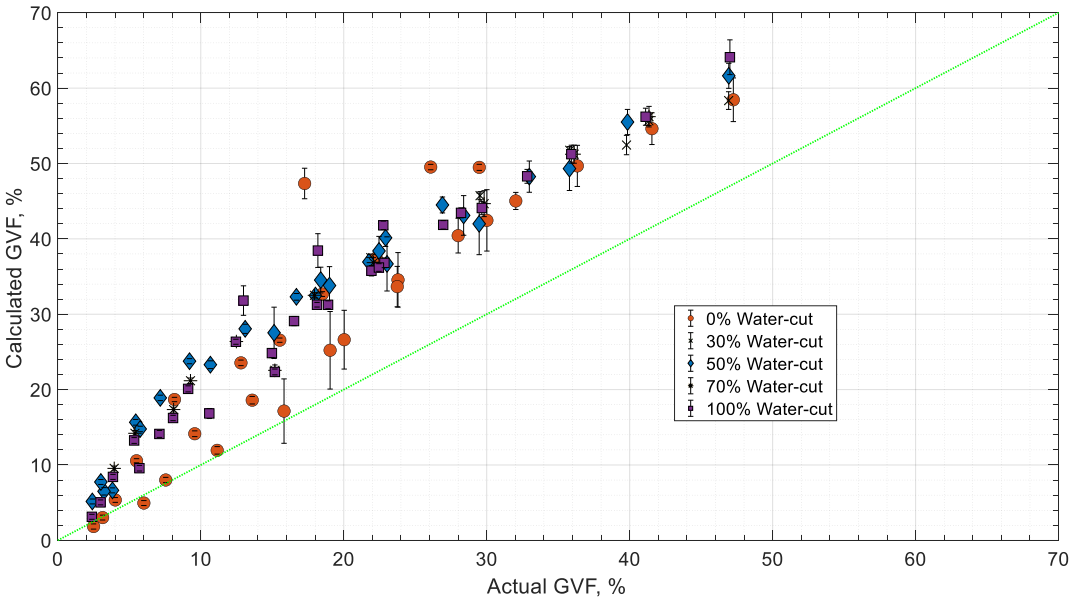

Fig. 9 – Calculated Vs. Actual GVF for All Water-Cuts

3.2 Error Modelling for Density at Second Frequency

The density error data presented thus far was all at the primary operating frequency of the meter. Fig. 10 shows the error in density measurements at 100% water-cut at the second frequency as a function of GVF. It is almost identical to the plot of error in the reported density at the primary frequency. However, unlike the error in density at the primary frequency, there are a few points where the density error is positive, only barely though.

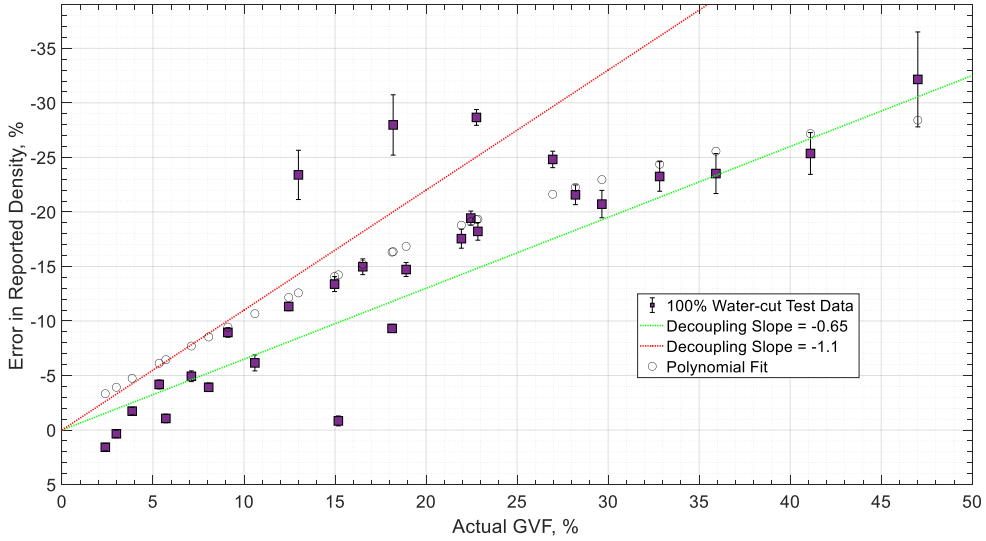

Fig. 10 – Error in Reported Density at Second Frequency vs. GVF

It is possible to dissect the error in density in the decoupling and compressibility terms to get a look at the contributions of each term. Fig. 11 and 12 shows the error in density at the primary and secondary frequencies respectively. As expected, the phase decoupling term dominates the error in the first frequency but the compressibility is expected to make a bigger contribution at the second frequency. However, as indicated by the manufacturer [5], the multi-frequency technology is mostly insensitive to the buoyancy error caused by free bubbles and it is only designed to handle trapped or suspended bubbles. It should be noted that free bubbles are typcially generated under laboratory conditions by injecting gas into a liquid flow. However, it has been observed in practice that suspended bubbles exist in many field applications, e.g. as a result of outgassing due to pressure drop. Nevertheless, it is good to see that the error in density follows the predictions from the Hemp model closely even though it is dominated by the phase decoupling term.

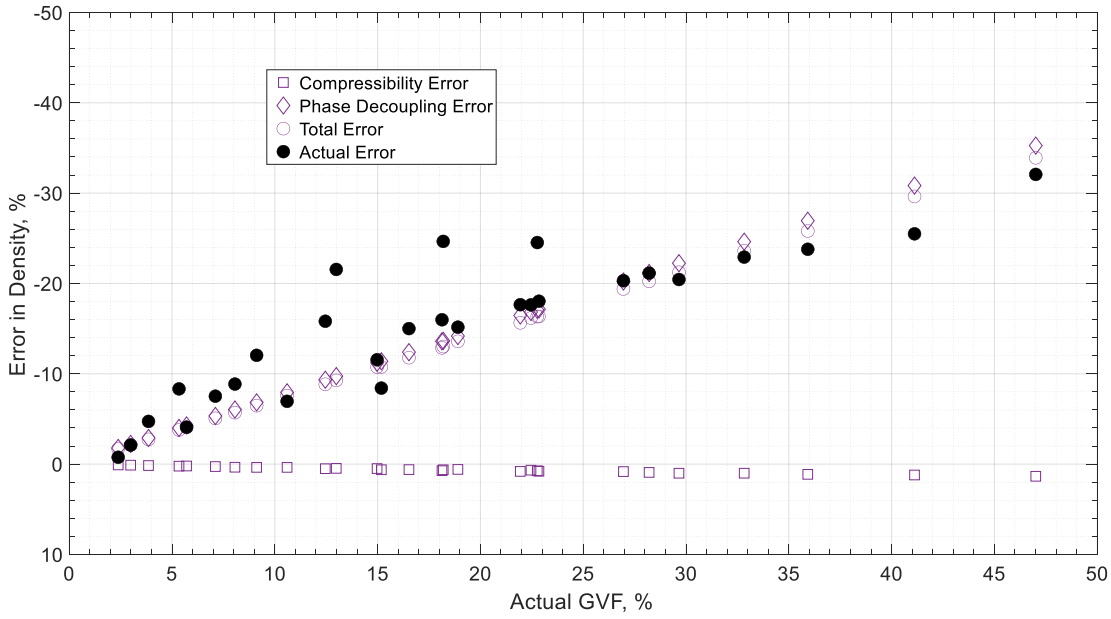

Fig. 11 – Density Error Decomposition at Primary Frequency and 100% Water-Cut

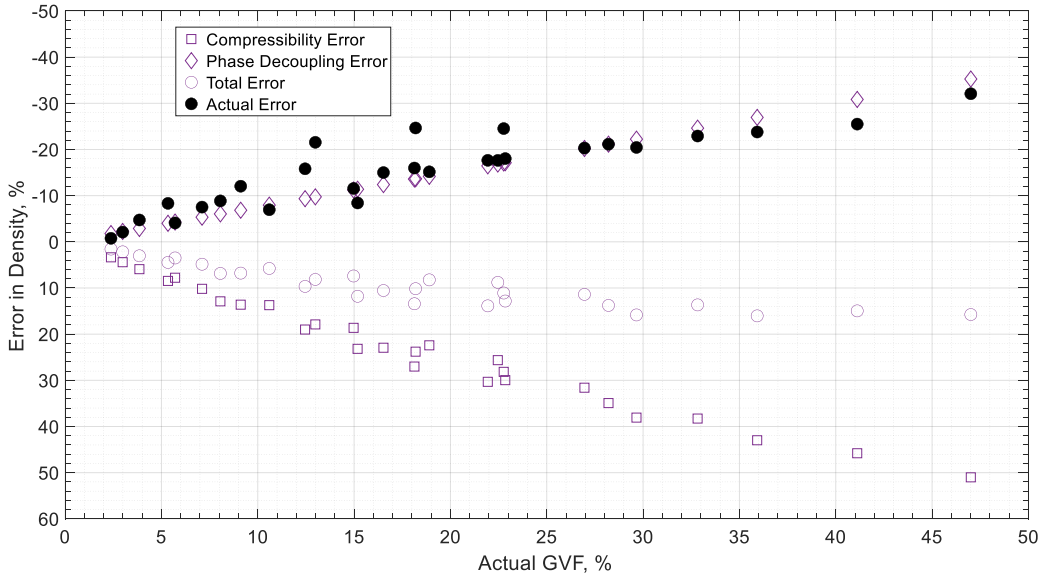

Fig. 12 – Density Error Decomposition at Secondary Frequency and 100% Water-Cut

3.3 Error Modelling for Mass Flow Rate

The error in mass flow rate is a much more involved – the two terms in Eqn. (2) are almost comparable. In fact, it is expected that phase decoupling (the first term) may dominate under GVF conditions and compressibility (the second term) may dominate under higher GVF conditions [9]. Indeed, this is the case as shown in Fig. 13 that plots the average error in mass flow rate at 0% water-cut as a function of GVF. Of course, given the higher scatter in measurements above 15% GVF, it is hard to say where the transition between positive and negative error occurs.

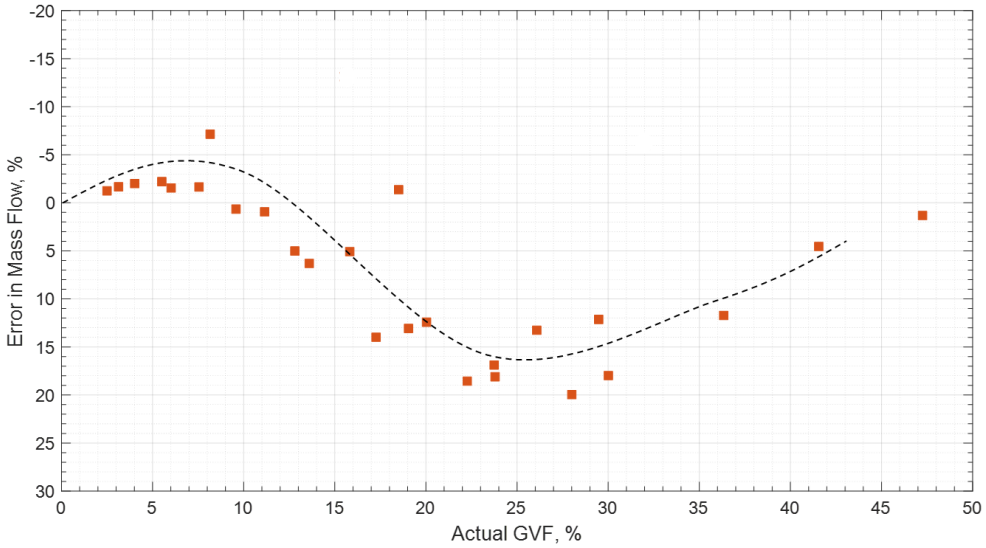

Fig. 13 – Average Error in Mass Flow Rate at 0% Water-Cut

In fact, the same behaviour is seen at 100% water-cut as well (Fig. 14).

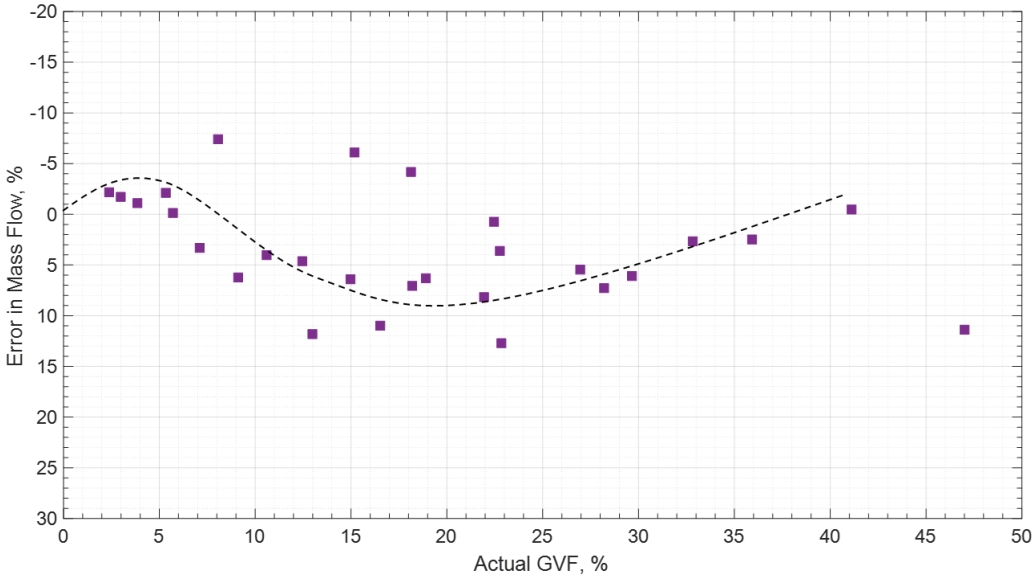

Fig. 14 – Average Error in Mass Flow Rate at 100% Water-Cut

Viewed from a different point of view, Fig. 15 shows the error in mass flow rate for 0% and 100% water-cut as a function of reported volumetric flow rate. It is clear that the error curve looks like a set of straight lines depending on the GVF.

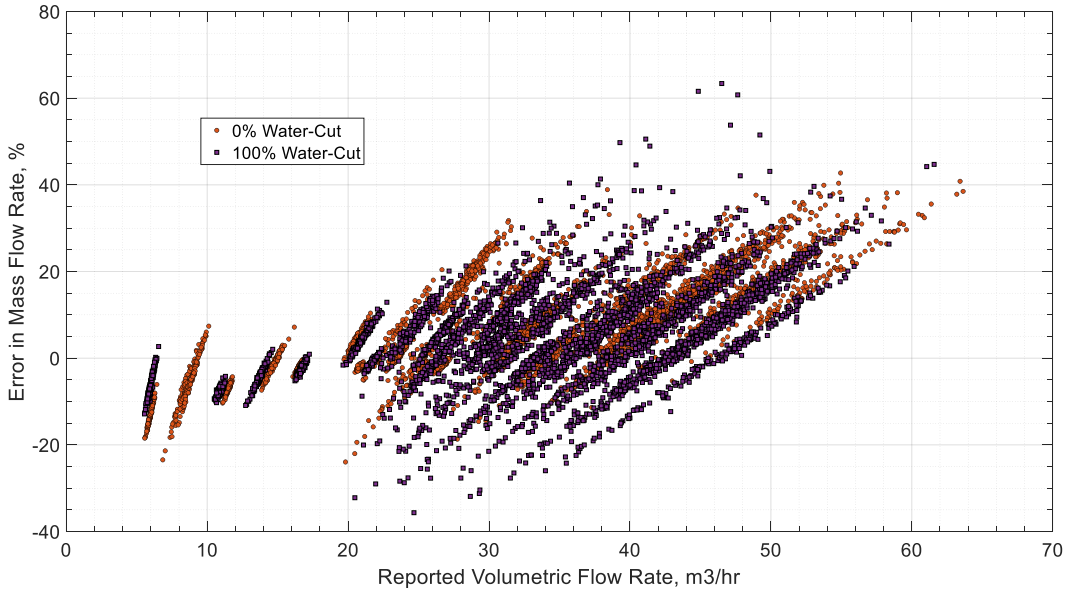

Fig. 15 – Error in Mass Flow Rate Vs. Reported Volumetric Flow Rate

One approach to achieve a fit is to force a curve fit on the Hemp model by adjusting the coefficients: -2 for phase decoupling term and 0.5 for the compressibility term. In fact, it turns that this approach does not provide very good predictions (Fig. 16). In fact, it reduces the error in original mass flow rate from the meter (yellow curve) by very little.

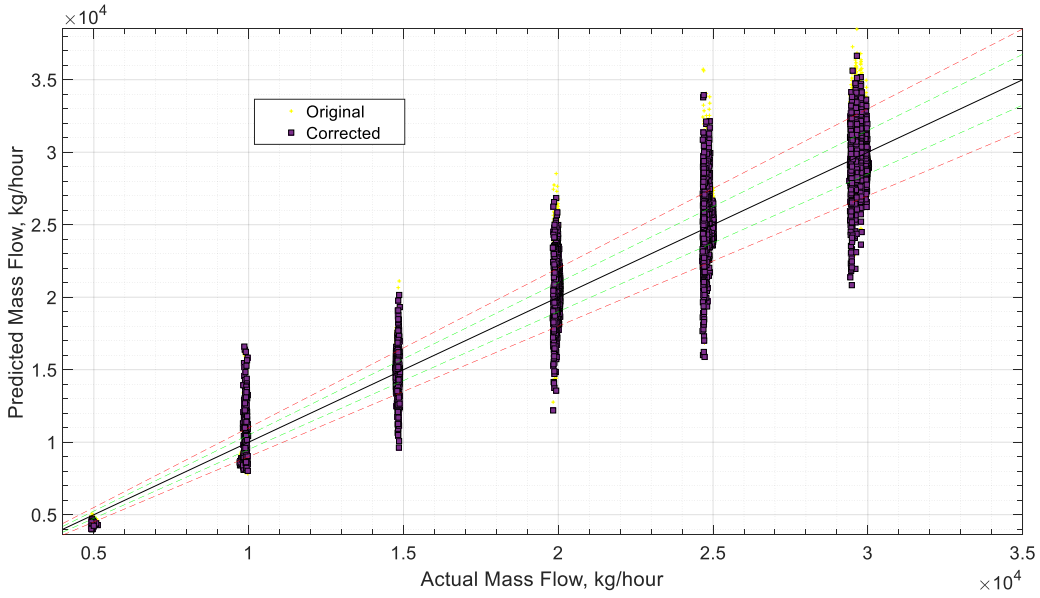

Fig. 16 – Predicted Mass Flow Rate from Hemp Model

4 NEURAL NETWORK MODELLING

Machine learning methods are ubiquitous today - from driverless cars to speech recognition to cancer detection. Due to the availability of cheap, large-scale computing and distributed storage, the use of these methods has proliferated across many engineering applications. Of course, such methods have been used to correct Coriolis meter measurements such as Henry [10] and Andrianov [11]. A neural network is simply an adaptive nonlinear dynamic system composed of a large

number of interconnected nodes or neurons. The network can process and tune itself to large data sets by adjusting the connections and weights between internal nodes and can result in very close predictions of system behaviour.

In order to analyze the data from the experiments, a neural network scheme shown in Fig. 17 was setup to analyse the test results.

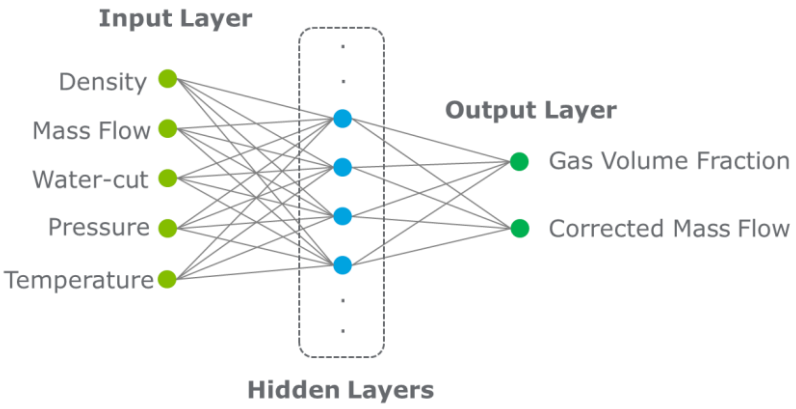

Fig. 17 – Neural Network Scheme

The number of hidden layers was adjusted from 2 to 50 and two algorithms – the Levenburg-Marquardt (LM) and the Bayesian regularization method were tried. Both these methods are simple backpropagation algorithms – the error in the predicted output is fed back and allocated through the network iteratively either for a preset number of iterations or until a certain goodness of fit is achieved. Unlike the use of the Hemp model, where individual a separate model may be developed for each water-cut separately, the neural network model was fed with the entire data set across all water-cuts. It was found that the neural network needed at least 60% of all the available data to be used for training in order to perform reasonably well. The remaining data was split evenly between validation and testing the model. The allocation of datasets between training, validation and testing was done using a random distribution method.

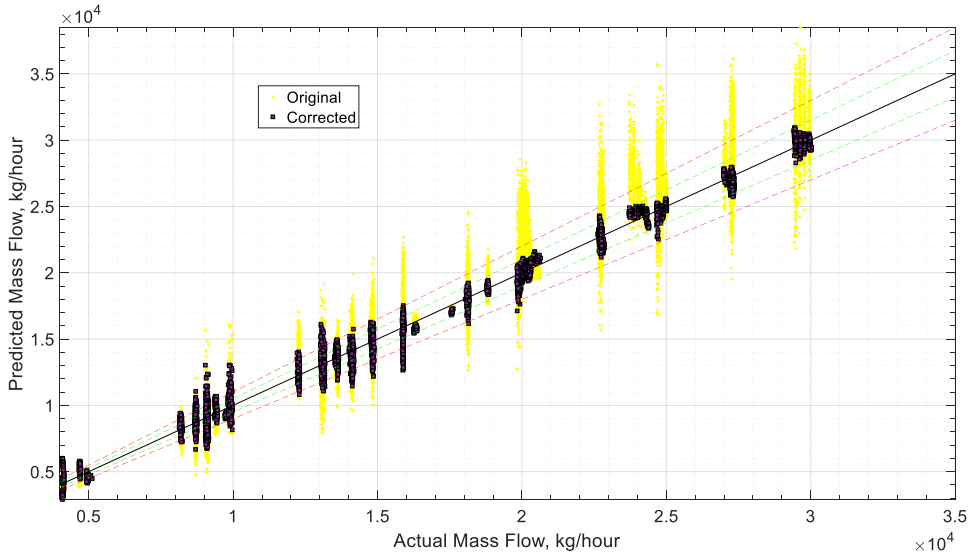

Fig. 18 – Performance of Neural Network Model with 2 Hidden Layers

Fig. 18 shows the results of the predictions from a network using the Bayesian regularization method with 2 hidden layers. While 90% of the predictions fell within a ±10% error bracket, only about 65% fell within a ±5% error bracket. Fig. 19 shows the results from a network with 5 hidden layers. It is marginally better, especially at the lower mass flow rates.

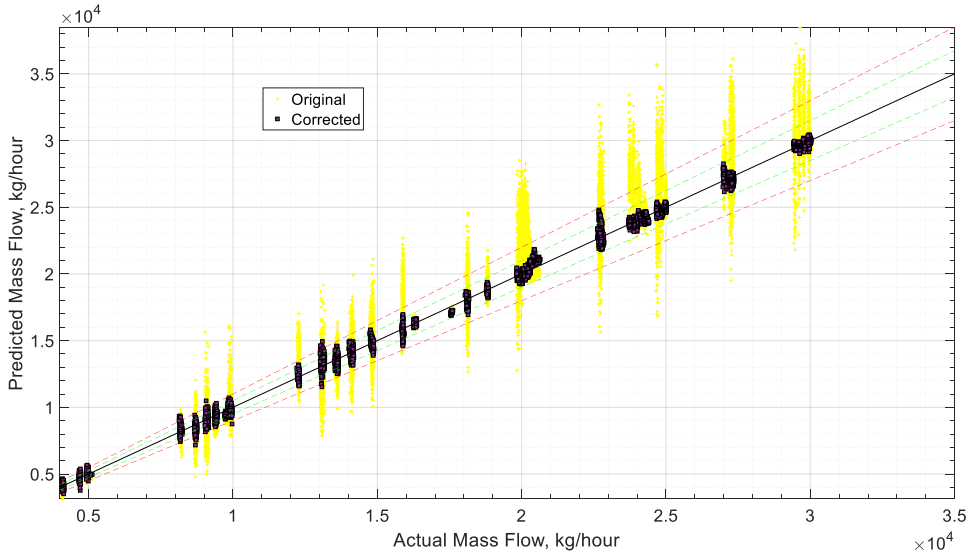

Fig. 19 – Performance of Neural Network Model with 5 Hidden Layers

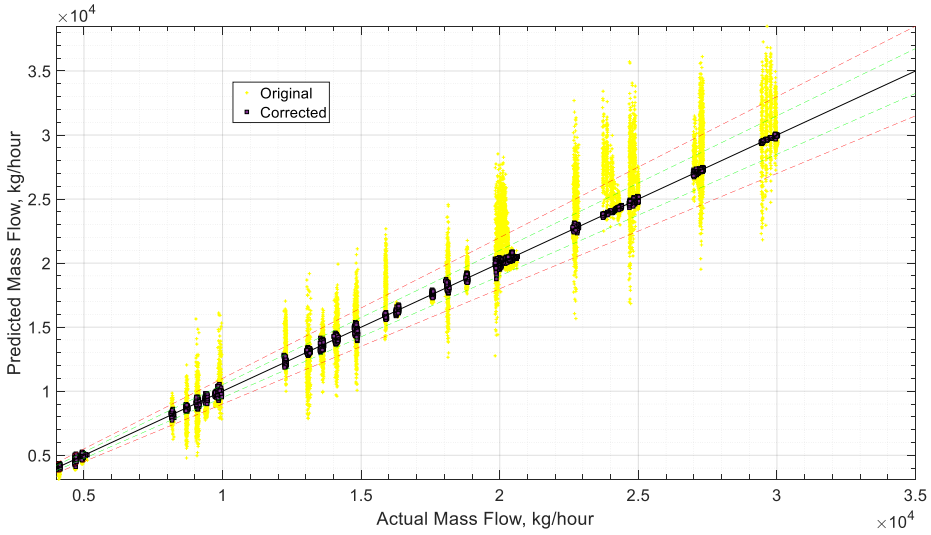

Fig. 20 – Performance of Neural Network Model with 20 Hidden Layers

Fig. 20 shows the performance of the model with 20 hidden layers where almost all the predictions fell within the ±5% error bracket. When the LM algorithm was used with 20 layers (Fig. 21), the predictions were marginally worse but most points still fell within the ±5% error bracket but the algorithm took approximately 25% less time to solve.

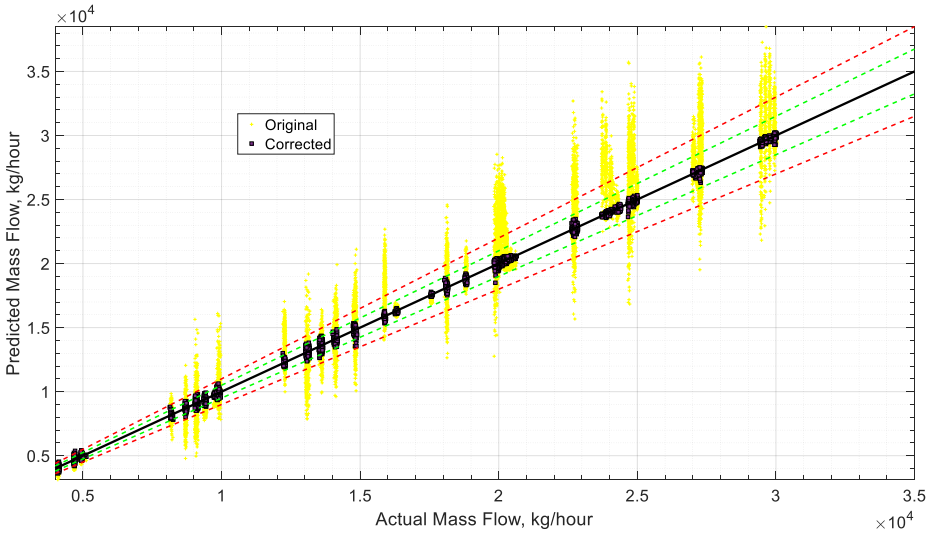

Fig. 21 – Performance of Neural Network Model with LM Algorithm

When the number of hidden layers was incresed to 50, the predicted results was almost on top of the actual results and it is likely that the model was overfitted. For practical purposes, 5 hidden layers would be more than sufficient to reduce the error in predicted measurements to within ±10%. Additional measurements may be used to reduce this error further to avoid excess dependance on the neural network model.

5 CONCLUSIONS

The multi-frequency Coriolis meter was tested under multiphase flow at 5 water-cuts and different liquid and gas flow rates. The test data showed that the meter performed well under no gas flow and was well within the uncertainty expected. Under flows with up to 15% GVF, while the measurements from the meter were reasonably good and the scatter in the measurements was within 5%. At GVF greater than 15%, both the scatter and error in the measurements from the meter increased. This is partly due to the uncertainty in the flow loop and the fact that the flow regime was likely to be slug flow at the meter. Nevertheless, the errors in the density and the mass flow were modelled using the theoretical framework developed by Hemp. While the errors in density were quite easily modelled and followed the theoretical model reasonably well, the error in mass flow rate showed considerable deviation. In fact, the predictions from the curve-fitting of the Hemp model for mass flow rate only marginally reduced the errors. A neural network model was also used to analyze the results from the test. The Bayesian regularization method with about hidden 20 layers reduced the predicted error in mass flow rate to be within a ±5%. The Levenburg-Marquardt (LM) algorithm was faster but marginally worse for the same number of hidden layers. A combination of a physics-based model for predicting GVF and a machine learning model for predicting mass flow rate may be a good combination to enable the use of Coriolis meters under multiphase flow.

6 NOTATION

α	Gas Volume Fraction
Ed	Error in Density
Em	Error in Mass Flow Rate
w1	Measured Frequency
b	Inner Diameter of Flow Tube
c	Speed of Sound

7 REFERENCES

[1] Shumakov, Y., Akbayev, B., Vigo, M., and Theuveny, B., "Five Years' Experience Using Coriolis Separators in North Sea Well Testing", Abu Dhabi International Petroleum Exhibition and Conference, Abu Dhabi, UAE, November 2014.

[2] H. Zhu, Application of Coriolis Mass Flowmeters in Bubbly and Particulate Two-Phase Flows, Shaker, 2009

[3] H. Zhu, A. Rieder and Y. Lin, "an innovative technology for Coriolis metering under entrained gas condition", Flomeko 2016, 2016.

[4] Zhu H, Rieder A, Drahm W, Lin Y, Guettler A, Wiesmann M, Hubensteiner J. From disturbance to measurement: Application of Coriolis for two-phase flow with gas bubbles. Flow Measurement and Instrumentation 79. 2021.

[5] Ceglia, P., and Ngo, H-T., "Entrained gas handling in Promass Coriolis Flowmeters", Endress+Hauser Flowtec AG White Paper, May 2020

[6] Hemp, J., and Kutin, J., "Theory of errors in Coriolis flowmeter readings due to compressibility of the fluid being metered", Flow Measurement and Instrumentation, 2006, Vol. 17, 359-369.

[7] Basse, N., "A review of the theory of Coriolis flowmeter measurement errors due to entrained particles", Flow Measurement and Instrumentation, 2014, Vol. 37, 107–118.

[8] Weinstein, J., "Multiphase Flow in Coriolis Mass Flow Meters – Error Sources and Best Practices", Proceedings of the North Sea Flow Measurement Workshop, 2010.

[9] Mahalingam, S., Yi,B., Okeke, N., Weidemann, P., and Lao, L., "Multiphase Metering Using a Coriolis Mass Flow Meter", Proceedings of the North Sea Flow Measurement Workshop, 2020.

[10] Henry MP, Tombs M, Duta MD, Zhou F, Mercado R, Kenyery F, "Two phase flow metering of viscous oil using a Coriolis mass flow meter: a case study", Flow Measurement and Instrumentation, 2006, Vol. 17, 399–413.

[11] Andrianov N., "A Machine Learning Approach for Virtual Flow Metering and Forecasting", IFAC Papers On Line, 2018, Vol. 51, 191-196.